

# Cross-Resolution Person Re-identification with Deep Antithetical Learning

Zijie Zhuang, Haizhou Ai, Long Chen, and Chong Shang

Tsinghua National Lab for Info. Sci. & Tech. (TNList),  
Department of Computer Science and Technology, Tsinghua University, Beijing,  
P.R.China, 100084  
jayzhuang42@gmail.com

**Abstract.** Images with different resolutions are ubiquitous in public person re-identification (ReID) datasets and real-world scenes, it is thus crucial for a person ReID model to handle the image resolution variations for improving its generalization ability. However, most existing person ReID methods pay little attention to this resolution discrepancy problem. One paradigm to deal with this problem is to use some complicated methods for mapping all images into an artificial image space, which however will disrupt the natural image distribution and requires heavy image preprocessing. In this paper, we analyze the deficiencies of several widely-used objective functions handling image resolution discrepancies and propose a new framework called deep antithetical learning that directly learns from the natural image space rather than creating an arbitrary one. We first quantify and categorize original training images according to their resolutions. Then we create an antithetical training set and make sure that original training images have counterparts with antithetical resolutions in this new set. At last, a novel Contrastive Center Loss(CCL) is proposed to learn from images with different resolutions without being interfered by their resolution discrepancies. Extensive experimental analyses and evaluations indicate that the proposed framework, even using a vanilla deep ReID network, exhibits remarkable performance improvements. Without bells and whistles, our approach outperforms previous state-of-the-art methods by a large margin.

**Keywords:** Person Re-identification · Image Resolution Discrepancies · Deep Antithetical Learning.

## 1 Introduction

Person re-identification (ReID) aims at identifying pedestrian identities across disjoint camera views. It suffers from various difficulties such as large variations of pose, viewpoint, and illumination conditions. Despite that person ReID tasks have been receiving increasing popularity, it remains a very challenging problem, especially in real-world application scenarios.

Recently, many inspiring works [1,34,38,16,33] have been proposed to tackle issues such as part misalignment and viewpoint changes. However, despite that



Fig. 1: Examples of images with different resolution in public datasets.

these models have achieved remarkable performance on several person ReID benchmarks, two obvious, but as yet, unanswered questions are seldom valued by these approaches: 1) does the image resolution discrepancies in the training set affect the performance of person ReID? and 2) how to prevent a model from being prone to certain resolution combinations when the training data reflects the natural image distribution partially. As shown in Fig. 1, the image resolution discrepancy problem is common in both public datasets and real-world applications. We argue that these discrepancies are caused by arbitrarily rescaling training images with different resolutions to a uniform size. The original resolutions of pedestrian image patches are diverse due to three reasons. First, the graphical perspective leads to various sizes of pedestrians in images. Second, configurations of surveillance cameras are different in both public datasets and real-world applications. Some old surveillance cameras can only produce low-resolution images while other modern cameras generate high-resolution images. Third, to the best of our knowledge, almost all deeply-learned ReID models require rescaling image patches to a uniform size in both training and testing. This procedure will inevitably lead to the image resolution discrepancy problem.

For a person ReID model, sufficient training data with different resolutions is vital for improving its generalization ability. For each image in the training set, if we get all its antithetical counterparts that have the same content but with different resolutions, it will help a ReID model to gain a better generalization ability. However, there is almost no chance of finding a pair of images in which the image from the low-resolution camera has a higher image resolution than the one from the high-resolution camera. It means that the resolution discrepancies in the actual training set are biased since certain resolution combinations are missing. Previous methods cover up this problem with carefully designed training hyperparameters [41,47,39,38,18] or sophisticated image pre-processing method [2]. Unlike these methods, we propose a generic and straightforward framework called deep antithetical learning that directly tackles the resolution discrepancy problem. The first step is the image quality assessment. Since the resolution changes of training images are mostly caused by manually rescaling images into a uniform size, we adopt the No-reference Image Quality assessment (NR-IQA) [35] and measure the image resolution in the frequency domain. In the second step, we generate an antithetical training set in which the resolution of images is antithetical to their counterparts in the original training set.

Image counterparts of lower resolutions can be easily generated by randomly downsampling, while approaches for enhancing the image resolution are limited. Generative adversarial networks (GANs) provide a practical approach for that purpose. However, neither CycleGAN [40] nor SRGAN [36] has the ability to enhance the image resolution to a specific level. Despite that we can split the original training set into multiple subsets, we cannot guarantee that every image has counterparts in every subset. Therefore, we roughly split the entire training set into two subsets: one with high-resolution (HR) images and another with low-resolution (LR) images. We then generate an antithetical training set in which the resolution of images is antithetical to their counterparts in the original training set. Specifically, for those HR images in the original set, we generate their LR counterparts by downsampling them randomly. And for those LR images in the original set, a GAN-based model is utilized for recovering fine texture details from them. These recovered images, along with the aforementioned manually blurred images, form the antithetical training set.

Apart from generating a new training set for better representing the natural image distribution, training the ReID model with proper objective functions is also crucial. We analyze the widely-used identification+verification paradigm [6] and find that the triplet loss with online hard negative mining (OHM) has a tendency to select training triplets of certain resolution combinations. This selection bias makes the ReID model suffer from resolution discrepancies and severely damages the performance. We address this problem by proposing a novel Contrastive Center Loss (CCL). The intuition behind is that rather than designing a sophisticated strategy for handling resolution differences between positive image pairs and negative ones, it is much easier to consider positive samples and negative samples separately. During the training procedure, the proposed CCL simultaneously clusters images of same identities and pushes the centers of different clusters away. To summarize, our contribution is three-fold:

- We focus on the image resolution discrepancy problem, which is seldom valued by previous methods as far as we know. We propose a training framework that produces antithetical images from the original training set and utilizes these images to eliminate biased discrepancies during the training phase.
- Unlike the previous super-resolution based ReID method [2], the goal of the proposed framework is to accommodate actual images whose resolution is naturally various. The proposed method does not require arbitrarily enhancing LR images during the test phase. Therefore, it has a potential to serve as a practical method for boosting many existing ReID methods.
- We go deep into the training procedure and investigate how the resolution discrepancies interfere with the triplet selection. The proposed Contrastive Center Loss shows an ability to learn discriminative features from images regardless of their various resolutions.

In conclusion, we present a high-performance person ReID system. Extensive experimental analyses and evaluations are conducted to demonstrate its effectiveness. Without bells and whistles, the proposed approach outperforms previous state-of-the-art methods on three large benchmarks by a large margin.

## 2 Related work

**Image Quality Assessment.** Image quality assessment (IQA) is an important research area. It can be accomplished in three ways: full reference image quality assessment (FR-IQA), reduced reference image quality assessment (RR-IQA), and no reference image quality assessment (NR-IQA). NR-IQA algorithms measure the quality of an image without the need for any reference image or its features. Recently, various strategies have been proposed to measure image quality, including edge detection [42], natural scene statistics [46], wavelet decomposition [44,45], and human visual system model [43]. In this work, since the rescaling procedure is the major source of visual degradation, we evaluate the resolution of images with their sharpness.

**Generative Adversarial Network.** Generative adversarial network (GAN) contains two sub-networks: a generator and a discriminator. The framework of GANs is first proposed by Goodfellow *et al.* [20]. After that, many researchers focus on improving the stability and visual quality of GANs [21,40,37]. In the field of computer vision, GANs are widely used in applications ranging from motion deblurring (DeblurGAN) [37] to texture recovering (SRGAN) [36]. To generate the antithetical training set, we adopt SRGAN [36] for recovering the fine texture details from low-quality images.

**Person Re-identification.** Person re-identification (ReID) can be split into two subproblems: feature representations and distance metric learning. Over the past decades, many studies focus on designing discriminative features [19,32,22,31], while others focus on constructing more robust metric learning algorithms [29,27,25]. With the rise of deep learning, deeply-learned models have dominated person ReID tasks. Several early works [1,3] take advantage of the two-stream siamese network and perform the pair-wise comparison in three steps: 1) extracting features from a given pair of images, 2) splitting feature cubes manually and comparing corresponding fractions across images, 3) determining whether these two images belong to the same identity. Attention-based methods [33,34] provide a more adaptive way for locating different human parts. Unlike these methods which focus on handling the variations of human pose and viewpoint changes, the proposed method tackles another common but crucial problem: the biased image resolution discrepancies in the training data.

## 3 Our approach

### 3.1 Framework

In person ReID tasks, the resolution of training images is naturally various. However, previous methods seldom value these resolution discrepancies. They probably learn biased mappings from these images. Besides, due to the fact that these discrepancies have significant impacts on distances between training images, some aggressive mining strategies such as online hard negative mining (OHM) will make the discrepancy problem even worse. To deal with these issues, we propose an approach to train the person ReID model directly from

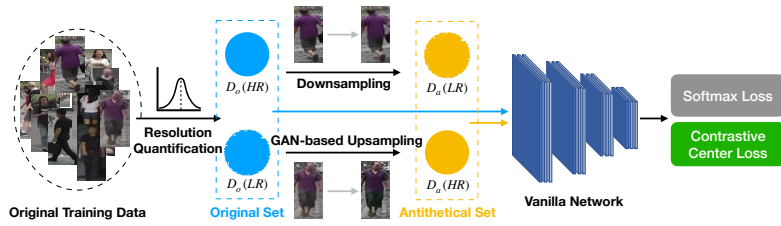


Fig. 2: The proposed training pipeline.

these images by deep antithetical learning. The motivations of the proposed deep antithetical learning are 1) producing antithetical training samples for balancing resolution discrepancies in the training set and 2) proposing a resolution-invariant objective function that produces better estimations of the image space. As demonstrated in Fig. 2, our approach mainly contains three steps. First, we measure the resolution of each image in training set with the sharpness metric. Second, we generate an antithetical training set by augmenting original low-resolution(LR) images with GANs and randomly downsampling original high-resolution(HR) images. In this antithetical training set, the resolution of each image is antithetical to that of its counterpart in the original training set. Third, after getting training samples from both the original training set and the antithetical set, we propose a novel Contrastive Center Loss (CCL) for learning relations between these images with various resolutions.

### 3.2 Evaluation of Original Training Set

The first step of generating the antithetical training set is to measure the resolution of images in the original training set. Person ReID tasks have two significant characteristics. 1) The standard image preprocessing pipeline does not change the brightness or hue of images but only their resolutions. 2) Images in ReID tasks are cropped image patches with tight bounding boxes, so the human body usually occupies a large portion of the entire image. The abundant texture information from the identity appearance provides rich evidence for measuring the image blurriness. We take advantage of the fact that sharper edges increase the high-frequency components and measure the resolution in the frequency domain.

We follow a simple sharpness metric proposed by Kanjar De *et al.* [30]. Given an image  $I$  of size  $h \times w$ , we first compute its Fourier transform representation  $F$ . Then we calculate the centered Fourier transform  $F_c$  of image  $I$  by shifting the origin of  $F$  to center. The threshold  $\tau$  is defined as the maximum absolute value of  $F_c$ . Now, we define the sharpness of an image  $I$  as:

$$\vartheta(I) = \frac{1}{h \times w} \sum_{i=1}^h \sum_{j=1}^w \mathbb{1}_{F_{i,j} \geq (\tau/1000)}, \quad (1)$$

where  $\mathbb{1}_{(condition)}$  represents the indicator function. After we obtain the sharpness of each image in the original training set  $D_o$ , we set up a threshold to split

the entire set into two subsets  $D_o(HR)$  and  $D_o(LR)$ . The reason for only splitting the set  $D_o$  into two subsets is that we lack the approach for tightly controlling the resolution of enhanced images. Even if we split  $D_o$  into multiple subsets, we cannot guarantee that the resolution of enhanced LR images reaches a specific level. We define this threshold as the mean sharpness of all images in the set  $D_o$ . The subset  $D_o(HR)$  contains images whose score is greater than this threshold, while images of inferior sharpness are collected into  $D_o(LR)$ .

### 3.3 Antithetical Training Set

As we mentioned above, images in the original training set  $D_o$  are different not only in pose, viewpoint, illumination conditions but also in the image resolution. Therefore, we propose to generate an antithetical training set  $D_a$  for counteracting the biased resolution discrepancies. In the previous section, we described how to quantify the image resolution and split the original training set into two subsets:  $D_o(HR)$  and  $D_o(LR)$ . Correspondingly, the antithetical training set  $D_a$  also contains two subsets:  $D_a(LR)$  and  $D_a(HR)$ .

For high-resolution images in the original subset  $D_o(HR)$ , the strategy for producing their antithetical low-resolution counterparts is straightforward. For each image, we first downsample this image by a factor which is randomly chosen from a uniform distribution  $\mathcal{U}(0.5, 0.8)$ , and then we rescale this image to its original size. These manually blurred images are denoted as  $D_a(LR)$ .

For low-resolution images in the original training set  $D_o(LR)$ , we adopt SRGAN [36], a GAN-based image super-resolution method, for recovering fine texture details from low-resolution images. For each image of size  $h \times w$  in  $D_o(LR)$ , SRGAN first upsamples it by a factor of 4 and then rescales this image to its original size. This rescaling procedure is necessary for eliminating random noises caused by SRGAN. In this way, we obtain the antithetical high-resolution subset  $D_a(HR)$ . For each low-resolution image in  $D_o(LR)$ , there is a corresponding high-resolution image in  $D_a(HR)$ . We will give a detailed evaluation in Section. 4.3.

### 3.4 Contrastive Center Loss and Deep Antithetical Learning

**Contrastive Center Loss.** The proposed Contrastive Center Loss (CCL) aims at estimating the distance between different images without being interfered by their resolution discrepancies. The softmax loss + triplet loss with online hard negative mining (trihard) approach is widely used in recent works. This paradigm prefers positive images with the maximum distance to the anchor and negative images with the minimum distance to the anchor. However, this paradigm neglects the fact that the resolution discrepancies have a salient influence on these distances (Fig. 3a). We find that in the actual training procedure, trihard tends to select positive image pairs of which the resolution is most different, and negative image pairs of which the resolution is most similar. This biased tendency keeps a ReID model trapped into the local optima and damages its generalization ability. We will give a more detailed analysis in Section. 4.5.

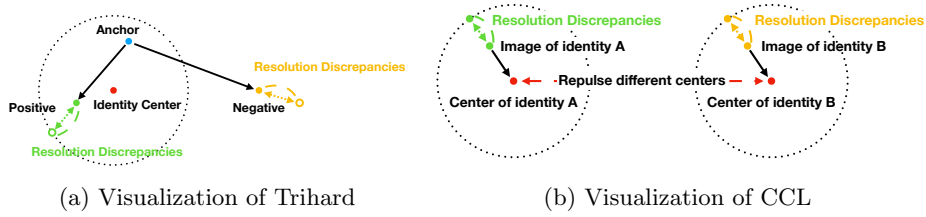


Fig. 3: Differences between trihard and the proposed CCL.

Fig. 3 shows the difference between the proposed CCL and the trihard loss. The trihard loss and the proposed CCL are both based on measuring distances between training samples. As we mentioned before, resolution discrepancies have a significant impact on these distances. For the trihard loss, resolution discrepancies in both positive samples and negative samples will affect the results of the loss function. To reduce the negative influence of resolution discrepancies, the proposed CCL measures intra-identity distances and inter-identity distances separately. For images of the same identity, we first estimate the center of each identity iteratively and minimize the distances between its center and corresponding image features:

$$\mathcal{L}_{intra} = \frac{1}{N} \sum_{i=1}^N \left(1 - \cos(f_i, C_{y_i})\right), \quad (2)$$

where  $f_i$  denotes the feature extracted from the  $i$ th image and  $C_{y_i}$  stands for the corresponding center. In this way, all features only connect to their corresponding identity centers, so that resolution discrepancies will not spread across different identities. For inter-identity distances, to make the most of negative images and avoid perturbations caused by resolution variations, we use negative samples indirectly. The relations of images of different identities are measured by the cosine distance of their corresponding centers. Since maximizing cosine distances is equivalent to minimizing their cosine similarities, the loss for repulsing different centers is defined as:

$$\mathcal{L}_{inter} = \frac{1}{N} \sum_{i=1}^N \sum_{j=1}^N \left| \cos(C_{y_i}, C_{y_j}) \right|, \quad (3)$$

where  $|\cdot|$  stands for the absolute value symbol. The reason for using the absolute value is that the orthogonality relation between identity centers is more discriminative than the positive/negative correlation. Note that both the intra-identity losses and the inter-identity losses are measured with cosine distances. An advantage of the cosine metric is that its range is certain. As shown in Table 5, inter-identity Euclidean distances are much greater than intra-identity distances. And during the training procedure, these two kinds of distances change at different speeds, and their corresponding losses change as well. Since these two losses

both rely on the trainable identity centers, it is important to keep them in a certain range. Finally, the Contrastive Center Loss (CCL) is formulated as:

$$\mathcal{L}_{LCC} = \alpha\mathcal{L}_{intra} + \beta\mathcal{L}_{inter}. \quad (4)$$

The weight  $\alpha$  and  $\beta$  for balancing losses will be discussed in Section. 4.5.

**Network Architecture.** We now describe the network for deep antithetical learning. With the help of the antithetical training set and the Contrastive Center Loss, even a vanilla deep network can achieve remarkable performance. We denote this deep network as ‘‘VanillaNet’’ in following sections. VanillaNet contains two basic components: 1) a convolutional network backbone with a global average pooling layer for extracting features, 2) two successive fully-connected layers denoted as  $FC_0$  and  $FC_1$ , where  $FC_1$  is used for ID classification. We use the standard Identification+Verification framework for training the VanillaNet. The cross entropy loss of ID classification can be formulated as follow:

$$\mathcal{L}_s(p, g) = - \sum_{k=1}^K \log(p_k) \mathbb{1}_{k=g}, \quad (5)$$

where  $\mathbb{1}_{(condition)}$  is the indicator function.  $p$  represents the prediction and  $g$  stands for the ground truth ID. The proposed CCL is connected to the last ReLU layer of the CNN backbone and the overall objective function for the proposed framework is formulated as:

$$\mathcal{L} = \mathcal{L}_s + \alpha\mathcal{L}_{intra} + \beta\mathcal{L}_{inter}. \quad (6)$$

During the training phase, we simply feed images from both original and antithetical training set into the network. In the testing phase, features from the last ReLU layer are used for ranking.

## 4 Experiments

### 4.1 Datasets

To evaluate the proposed framework, we select three public datasets: Market-1501 [14], Duke-MTMC-reID [13], and CUHK03 [12].

**CUHK03.** The CUHK03 dataset contains 14096 images of 1467 identities. There are at most ten images for each identity shot by two disjoint cameras. Unlike previous testing protocol which only adopts 100 identities for testing, we follow the new protocol presented by Zhong *et al.* [28]. This new protocol adopts 767 identities for training and the rest 700 identities for testing. Under this protocol, each identity has more than one ground truth image in the gallery, which is more consistent with the real-world applications.

**Market-1501.** The Market-1501 dataset is a large ReID dataset which contains 32643 annotated boxes of 1501 different identities. We divide this dataset into a training set of 750 identities and a testing set of 751. Since images in

this dataset are collected by the pedestrian detector, it involves several detector failures. Besides, the quality of images shot by one particular camera is significantly lower than the quality of other images. These two characteristics make this dataset suitable for quantifying the effectiveness of the proposed method.

**Duke-MTMC-reID.** Duke-MTMC-reID is a newly published dataset. It contains 36411 bounding boxes shot by 8 different cameras. We use 16522 training images of 702 identities, leaving 2228 query images of the other 702 identities and 17661 gallery images for the testing procedure. Unlike Market-1501, the quality of images in this dataset is much higher and more consistent.

## 4.2 Implementation Details

For the SRGAN, we use the same training parameters provided in its original paper [36]. We first train the model on the DIV2K dataset and then fine-tune it on HR images from the ReID training set. In the training phase, rather than cropping training images randomly, we directly pad HR training images with zeros and resize them to the target scale.

For the VanillaNet, we adopt the ResNet-50 [5] backbone in all experiments. The batch size is set to 60. Both the weight  $\alpha$  and  $\beta$  are set to 0.1 and the output dimension of the CNN backbone is 2048. In both training and testing phase, all images are resized to the size of  $256 \times 128$ . The data augmentation includes RandomErasing [26] and random horizontal flipping. To train the model, we adopt stochastic gradient descent (SGD) [24] optimizer with an initial learning rate of 0.01 and weight decay of  $5 \times 10^{-4}$ . In all experiments, the training phase lasts for 60 epochs. And the learning rate starts to decay exponentially at 20th epoch with the base of 0.1. The overall time cost of training the proposed model is minor. For the Market-1501, it takes about 130 minutes for the training procedure on a single GTX-Titan-Xp GPU.

## 4.3 Quantifying Image Resolution

In this section, we analyze image resolution distributions of all datasets. Since two subsets of CUHK03 are similar in human pose, viewpoint, and illumination conditions, we only present histograms of the “detected” subset. As shown in Fig.4, diagrams in each column correspond to Market-1501, Duke-MTMC-reID, and CUHK03 (detected), respectively. Histograms in the first row represent the resolution distribution of the original training set  $D_o$ . And the red dashed line in each of them is the threshold for splitting the original set. In the second row, we compare the resolution of images in the original LR set  $D_o(LR)$  and its corresponding antithetical set  $D_a(HR)$ . The blue histogram in each diagram corresponds to  $D_o(LR)$ , and the orange one corresponds to  $D_a(HR)$ . We also present the statistical analyses in Table 1 and some examples in Fig. 5.

In summary, for Market-1501, Duke-MTMC-reID, and CUHK03 (labeled), SRGAN can significantly augment low-resolution images in the original training set, especially under low light conditions.

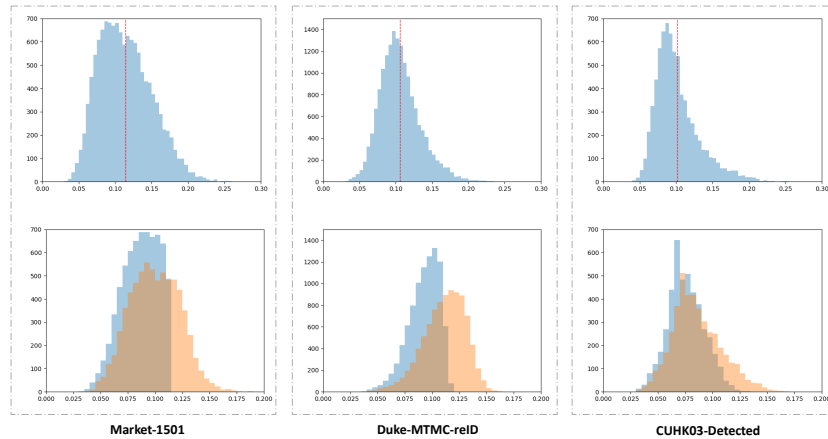


Fig. 4: Visualizations of the image resolution in different datasets.

Datasets	original set $D_o(LR)$			antithetical set $D_a(HR)$		
	num	mean	median	num	mean	median
Market-1501	6906	0.087	0.091	6906	0.100	0.102
Duke-MTMC-reID	9121	0.093	0.075	9121	0.111	0.089
CUHK03 (labeled)	4661	0.075	0.088	4661	0.085	0.101
CUHK03 (detected)	4444	0.076	0.066	4444	0.086	0.070

Table 1: Quantifying the mean and median of image sharpness scores before and after enhancements. Both the mean and median sharpness scores of low-resolution images are improved.

#### 4.4 Analyzing Different Data Fusion Strategies

The antithetical training set  $D_a$  is produced by two different approaches: enhancing LR images with SRGAN and downscaling HR images randomly. This specific strategy seems unsymmetrical. In this section, we demonstrate that both strategies are crucial for better estimating the real-world distribution. All following experiments are conducted on the test set of Market-1501. We first evaluate whether the antithetical training set improves the ReID performance. Only softmax identification loss is applied to VanillaNet in these experiments. As shown in Table 2, both the enhanced set  $D_a(HR)$  and the decayed set  $D_a(LR)$  are beneficial to the ReID performance. When combining  $D_a(HR)$ ,  $D_a(LR)$ , and  $D_o$  together, VanillaNet reaches the highest performance.

Following the same criterion for splitting the training set, we further divide all query images into high-resolution probes and low-resolution probes. As shown in Table 3, the performance of querying with LR probes is much lower than that of querying with HR probes. Furthermore, we notice significant improvements in both LR queries and HR queries when adopting the antithetical training set. These results indicate that the ReID model benefits from not only the SRGAN



Fig. 5: Examples of low-resolution images in the original training set and their counterparts in the antithetical set.

Datasets	rank-1	mAP
$D_o$	88.63	72.47
$D_o+D_a(LR)$	89.16	73.98
$D_o+D_a(HR)$	89.84	73.75
$D_o+D_a$	<b>90.11</b>	<b>74.33</b>

Table 2: Comparing training data.

Probe	$D_o$		$D_o+D_a$	
	rank-1	mAP	rank-1	mAP
LR	85.48	68.95	87.25	70.86
HR	92.26	76.54	93.41	78.33
ALL	88.63	72.47	90.11	74.33

Table 3: Comparing query probe.

but also the random downsampling procedure. To further prove this conclusion, we compare the performance of our data augmentation approach with the other two approaches: 1) enhancing all images in  $D_o$  and 2) downsampling all these images. Table 4 demonstrates the performance of these approaches and internal differences on image distances. Note that these experiments are conducted with both the softmax loss and the proposed CCL for clustering images and tracking the identity centers.  $D_{intra}$  and  $D_{inter}$  stand for the average distance between images of the same identity, images of different identities on the test set.  $D_{centers}$  represents the average distance between all identity centers on the training set. We adopt  $D_{centers}$  for measuring the separation of different identity clusters.

Compared to other two fusion strategies, VanillaNet with the proposed CCL and antithetical set obtains the smallest intra-identity distances and the largest center distances. These results indicate that VanillaNet gains a better generalization ability on the test set with the proposed CCL and antithetical images.

Data Fusion Strategy	rank-1	mAP	$D_{intra}$	$D_{inter}$	$D_{centers}$
Original+All SRGAN	89.85	74.66	0.4559	0.8075	0.6100
Original+All Downscale	87.14	72.47	0.4590	<b>0.8257</b>	0.6085
Original+Our Approach	<b>90.83</b>	<b>76.63</b>	<b>0.4548</b>	0.8127	<b>0.6122</b>

Table 4: Comparing fusion strategies ( $\alpha = 0.1, \beta = 0.1$ ).

#### 4.5 Comparing CCL with Other Objective Functions

In this section, we will discuss the differences between triplet loss with OHM (trihard), Center Loss, and the proposed Contrast Center Loss(CCL).

For trihard, our experiments indicate that the resolution of training images has biased influences on the triplet-picking procedure. Given a probe image, trihard expects the farthest image of the same identity and the nearest image of a different identity. As shown in Table 5, when the probe is with low-resolution, it is more likely for trihard to pick a positive HR image and a negative LR image at the same time. We also track all selected triplets during the training phase. Histograms in Fig. 6 show the possibility of picking image pairs with certain resolution combinations. The selected positive images tend to have a most different resolution than that of probe images, while the resolution of picked negative images tends to be the same as that of probe images. In a word, trihard suffers from resolution discrepancies and fails to learn all possible image combinations.

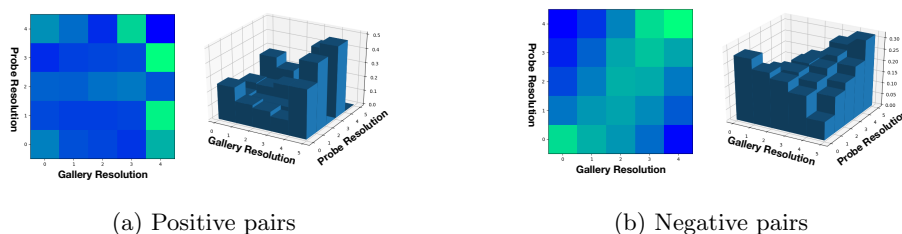


Fig. 6: The selection tendency of TriHard. Picked positive image pairs usually have the biggest difference in resolution, while the negative pairs have the most similar resolution. These histograms are normalized along the gallery axis.

Distance between selected image pairs	intra-identity	inter-identity
(sharp, sharp)	0.2580	0.7306
(blur, blur)	0.2475	0.7182
(sharp, blur) and (blur, sharp)	0.2754	0.7255

Table 5: Distances between images with different resolutions (Training Set).

For the Center Loss, the resolution discrepancy problem is much less severe. Images are only used for estimating their corresponding identity centers, so the discrepancies will not spread across different identities. However, it is at the cost of ignoring all negative images. Unlike Center Loss, the proposed CCL manages to learn from negative samples indirectly. When updating identity centers, the proposed CCL not only reduces the distance between image features and their

corresponding center but also pushes different centers away. In this way, images are connected to their relevant centers directly and irrelevant centers indirectly. As shown in Table 6, the proposed CCL significantly increases the distances between different centers and distances between images of different identity. At the same time, the average intra-identity distance is slightly larger.

Data Fusion Strategy	rank-1	mAP	$D_{intra}$	$D_{inter}$	$D_{centers}$
Softmax	90.11	74.33	0.4110	0.6880	-
Softmax+Center Loss	90.29	75.00	<b>0.3295</b>	0.547	0.3893
Softmax+Contrastive Center Loss	<b>90.83</b>	<b>76.63</b>	0.4548	<b>0.8127</b>	<b>0.6122</b>

Table 6: Compare Center Loss and the proposed CCL.

alpha	beta	rank-1	mAP	$D_{intra}$	$D_{inter}$
1	1	83.49	61.7	0.4729	1.1591
1	0.1	90.2	75.56	0.2294	0.413
0.1	0.1	<b>90.83</b>	<b>76.63</b>	0.4548	0.8127
0.1	0.01	90.44	75.36	0.3806	0.6525
0.01	0.01	90.38	76.07	0.4168	0.7093

Table 7: Effect of different parameters on Market-1501.

#### 4.6 Comparing with State-of-the-Art

According to Table 7, we set  $\alpha = 0.1$  and  $\beta = 0.1$  in all following experiments. We now compare our results with other state-of-the-art methods in Table 8 and 9. With the single-query settings, our model achieves 90.8% rank-1 accuracy and 76.6% mAP on Market-1501. On Duke-MTMC-reID, compared to the previous best model, we achieve an absolute improvement of 3.7% in rank-1 and 6.7% in mAP. On CUHK03, the proposed model achieves 62.5% rank-1 accuracy / 62.7% mAP on CUHK03 (labeled), and 55.9% rank-1 accuracy / 55.0% mAP on CUHK03 (detected). Another observation is that the performance on all datasets can be boosted by simply adopting a more powerful network, such as ResNet-101. Therefore, it has a potential to serve as a practical method for boosting many existing ReID methods.

## 5 Conclusions

In this paper, we analyze the ubiquitous image resolution discrepancy problem in person ReID tasks. Extensive experiments indicate that these discrepancies

Methods	Market-1501				Duke			
	rank-1	rank-5	rank-10	mAP	rank-1	rank-5	rank-10	mAP
Re-rank [28]	77.1	-	-	63.6	-	-	-	-
LSRO [11]	84.0	-	-	66.1	67.7	-	-	47.1
TriNet [10]	84.9	94.2	-	69.1	-	-	-	-
SVDNet [18]	82.3	92.3	95.2	62.1	76.7	86.4	89.9	56.8
DPFL [16]	88.6	-	-	72.6	79.2	-	-	60.6
Ours(ResNet50)	90.8	<b>96.9</b>	<b>98.0</b>	76.6	82.9	91.9	93.8	67.3
Ours+Rerank	<b>92.7</b>	95.8	97.2	<b>89.1</b>	<b>87.4</b>	<b>92.5</b>	<b>94.6</b>	<b>83.2</b>
Ours(ResNet101)	91.5	96.8	97.7	79.5	84.5	92.6	94.3	70.1

Table 8: Results on Market1501 and Duke-MTMC-reID in single query mode.

Methods	CUHK03 (labeled)		CUHK03 (detected)	
	rank-1	mAP	rank-1	mAP
IDE+DaF [8]	27.5	31.5	26.4	30.0
PAN [15]	36.9	35.0	36.3	34.0
DPFL [16]	43.0	40.5	40.7	37.0
SVDNet [18]	40.9	37.8	41.5	37.3
TriNet [10]	58.1	53.8	55.5	50.7
Ours(ResNet50)	62.5	62.7	55.9	55.0
Ours+Rerank	<b>68.3</b>	<b>69.5</b>	<b>59.6</b>	<b>61.6</b>
Ours(ResNet101)	68.9	68.7	58.6	59.0

Table 9: Results on CUHK03 (labeled) and CUHK03 (detected).

have a negative impact on the ReID performance, and some mining strategies such as OHM will make this problem even worse. In this paper, we propose a novel training framework called deep antithetical learning and address this issue in two steps. First, an additional antithetical training set is generated for balancing biased resolution discrepancies. Second, we propose a resolution-invariant objective function called Contrastive Center Loss. Experiments demonstrate that even using a vanilla ReID network, the proposed framework outperforms previous state-of-the-art methods by a large margin.

## References

1. Li, W., Zhao, R., Xiao, T., Wang, X.: Deepreid: Deep filter pairing neural network for person re-identification. In: CVPR. (2014)
2. Jiao, J., Zheng, W.S., Wu, A., Zhu, X., Gong, S.: Deep low-resolution person re-identification. In: AAAI. (2018)
3. Ahmed, E., Jones, M., Marks, T.K.: An improved deep learning architecture for person re-identification. In: CVPR. (2015)
4. Hadsell, R., Chopra, S., LeCun, Y.: Dimensionality reduction by learning an invariant mapping. In: CVPR. (2006)

5. He, K., Zhang, X., Ren, S., Sun, J.: Deep residual learning for image recognition. In: CVPR. (2016)
6. Zheng, Z., Zheng, L., Yang, Y.: A discriminatively learned cnn embedding for person reidentification. ACM TOMM (2017)
7. Wen, Y., Zhang, K., Li, Z., Qiao, Y.: A discriminative feature learning approach for deep face recognition. In: ECCV. (2016)
8. Yu, R., Zhou, Z., Bai, S., Bai, X.: Divide and fuse: A re-ranking approach for person re-identification. arXiv preprint arXiv:1708.04169 (2017)
9. Xie, S., Girshick, R., Dollár, P., Tu, Z., He, K.: Aggregated residual transformations for deep neural networks. In: CVPR. (2017)
10. Hermans, A., Beyer, L., Leibe, B.: In defense of the triplet loss for person re-identification. arXiv preprint arXiv:1703.07737 (2017)
11. Zheng, Z., Zheng, L., Yang, Y.: Unlabeled samples generated by gan improve the person re-identification baseline in vitro. arXiv preprint arXiv:1701.07717 **3** (2017)
12. Li, W., Zhao, R., Xiao, T., Wang, X.: Deepreid: Deep filter pairing neural network for person re-identification. In: CVPR. (2014)
13. Zheng, Z., Zheng, L., Yang, Y.: Unlabeled samples generated by gan improve the person re-identification baseline in vitro. In: ICCV. (2017)
14. Zheng, L., Shen, L., Tian, L., Wang, S., Wang, J., Tian, Q.: Scalable person re-identification: A benchmark. In: ICCV. (2015)
15. Zheng, Z., Zheng, L., Yang, Y.: Pedestrian alignment network for large-scale person re-identification. arXiv preprint arXiv:1707.00408 (2017)
16. Chen, Y., Zhu, X., Gong, S.: Person re-identification by deep learning multi-scale representations. In: CVPR. (2017)
17. Liao, S., Hu, Y., Zhu, X., Li, S.Z.: Person re-identification by local maximal occurrence representation and metric learning. In: CVPR. (2015)
18. Sun, Y., Zheng, L., Deng, W., Wang, S.: Svdnet for pedestrian retrieval. In: CVPR. (2017)
19. Ojala, T., Pietikainen, M., Maenpaa, T.: Multiresolution gray-scale and rotation invariant texture classification with local binary patterns. PAMI **24** (2002) 971–987
20. Goodfellow, I., Pouget-Abadie, J., Mirza, M., Xu, B., Warde-Farley, D., Ozair, S., Courville, A., Bengio, Y.: Generative adversarial nets. In: NIPS. (2014)
21. Radford, A., Metz, L., Chintala, S.: Unsupervised representation learning with deep convolutional generative adversarial networks. arXiv preprint arXiv:1511.06434 (2015)
22. Farenzena, M., Bazzani, L., Perina, A., Murino, V., Cristani, M.: Person re-identification by symmetry-driven accumulation of local features. In: CVPR. (2010)
23. Li, D., Chen, X., Zhang, Z., Huang, K.: Learning deep context-aware features over body and latent parts for person re-identification. In: CVPR. (2017)
24. Bottou, L.: Large-scale machine learning with stochastic gradient descent. In: COMPSTAT. (2010)
25. Koestinger, M., Hirzer, M., Wohlhart, P., Roth, P.M., Bischof, H.: Large scale metric learning from equivalence constraints. In: CVPR. (2012)
26. Zhong, Z., Zheng, L., Kang, G., Li, S., Yang, Y.: Random erasing data augmentation. arXiv preprint arXiv:1708.04896 (2017)
27. Yi, D., Lei, Z., Liao, S., Li, S.Z.: Deep metric learning for person re-identification. In: ICPR. (2014)
28. Zhong, Z., Zheng, L., Cao, D., Li, S.: Re-ranking person re-identification with k-reciprocal encoding. In: CVPR. (2017)
29. Davis, J.V., Kulis, B., Jain, P., Sra, S., Dhillon, I.S.: Information-theoretic metric learning. In: ICML. (2007)

30. De, K., Masilamani, V.: Image sharpness measure for blurred images in frequency domain. *Procedia Engineering* **64** (2013) 149–158
31. Zhao, R., Ouyang, W., Wang, X.: Unsupervised salience learning for person re-identification. In: *CVPR*. (2013)
32. Yang, Y., Yang, J., Yan, J., Liao, S., Yi, D., Li, S.Z.: Salient color names for person re-identification. In: *ECCV*. (2014)
33. Liu, H., Feng, J., Jie, Z., Jayashree, K., Zhao, B., Qi, M., Jiang, J., Yan, S.: Neural person search machines. In: *ICCV*. (2017)
34. Zhao, L., Li, X., Zhuang, Y., Wang, J.: Deeply-learned part-aligned representations for person re-identification. In: *CVPR*. (2017)
35. De, K., Masilamani, V.: Image sharpness measure for blurred images in frequency domain. *Procedia Engineering* **64** (2013) 149–158
36. Ledig, C., Theis, L., Huszar, F., Caballero, J., Cunningham, A., Acosta, A., Aitken, A., Tejani, A., Totz, J., Wang, Z., et al.: Photo-realistic single image super-resolution using a generative adversarial network. In: *CVPR*. (2017)
37. Kupyn, O., Budzan, V., Mykhailych, M., Mishkin, D., Matas, J.: Deblurgan: Blind motion deblurring using conditional adversarial networks. *arXiv preprint arXiv:1711.07064* (2017)
38. Sun, Y., Zheng, L., Yang, Y., Tian, Q., Wang, S.: Beyond part models: Person retrieval with refined part pooling. *arXiv preprint arXiv:1711.09349* (2017)
39. Zhang, X., Luo, H., Fan, X., Xiang, W., Sun, Y., Xiao, Q., Jiang, W., Zhang, C., Sun, J.: Alignedreid: Surpassing human-level performance in person re-identification. *arXiv preprint arXiv:1711.08184* (2017)
40. Zhu, J.Y., Park, T., Isola, P., Efros, A.A.: Unpaired image-to-image translation using cycle-consistent adversarial networks. In: *CVPR*. (2017)
41. Xiao, Q., Luo, H., Zhang, C.: Margin sample mining loss: A deep learning based method for person re-identification. *arXiv preprint arXiv:1710.00478* (2017)
42. Marziliano, P., Dufaux, F., Winkler, S., Ebrahimi, T.: Perceptual blur and ringing metrics: application to jpeg2000. *Signal processing: Image communication* **19** (2004) 163–172
43. Du, J., Yu, Y., Xie, S.: A new image quality assessment based on hvs. *Journal of Electronics (China)* **22** (2005) 315–320
44. Sheikh, H.R., Bovik, A.C., Cormack, L.: No-reference quality assessment using natural scene statistics: Jpeg2000. *TIP* **14** (2005) 1918–1927
45. Chen, M.J., Bovik, A.C.: No-reference image blur assessment using multiscale gradient. *EURASIP Journal on image and video processing* **2011** (2011) 3
46. Brandão, T., Queluz, M.P.: No-reference image quality assessment based on dct domain statistics. *Signal Processing* **88** (2008) 822–833
47. Hermans, A., Beyer, L., Leibe, B.: In defense of the triplet loss for person re-identification. *arXiv preprint arXiv:1703.07737* (2017)